JOURNAL OF THERMOPHYSICS AND HEAT TRANSFER
Vol. 16, No. 2, April–June 2002

Numerical Simulation of Gas Flow over Microscale Airfoils

Quanhua Sun* and Iain D. Boyd†
University of Michigan, Ann Arbor, Michigan 48109
and
Graham V. Candler‡
University of Minnesota, Minneapolis, Minnesota 55455

Flows over microscale airfoils are investigated using both particle and continuum approaches. An implementation of the information preservation technique based on the direct simulation Monte Carlo method is used to simulate flows over a flat plate of zero thickness at low Reynolds number ($Re < 1 \times 10^2$), and good agreement is obtained comparing with experimental data and theoretical results. Investigation shows that the aerodynamics of a flat plate with thickness ratio of 5% at $Re = 4$ is quite different from that at $Re = 4 \times 10^3$ that were measured experimentally. A continuum approach with slip boundary conditions predicts a similar basic flow pattern as the information preservation method with differences in details, which may indicate that continuum approaches are not suitable for this kind of flow because of rarefied effects.

Nomenclature

C	=	thermal velocity of particles
C_D	=	drag coefficient
C_f	=	skin friction
Kn	=	Knudsen number
k	=	Boltzmann constant
L	=	physical dimension
M	=	Mach number
m	=	mass of molecules
N	=	sampling size
N_c	=	number of particles in computational cells
n	=	number density
p	=	pressure
R	=	specific gas constant
Re	=	Reynolds number
s	=	normalized velocity
T	=	temperature
t	=	time
V	=	velocity
x, y, z	=	physical location
γ	=	Euler constant, 0.57722,. . .
Δt	=	time step
θ	=	accommodation coefficient
κ	=	slip coefficient
λ	=	mean free path
μ	=	viscosity of gases
ρ	=	density of gases
σ	=	physical statistical scatter
σ'	=	numerical statistical scatter
τ	=	shear stress
υ	=	specific volume

Subscripts and Superscripts

c	=	cell information
i	=	incident state
r	=	reflect state
s	=	surface
t	=	component parallel to the surface
w	=	wall surface
x, y, z	=	component in x, y, or z direction
1, 2	=	particles 1 and 2 in a collision pair
3	=	component normal to the surface
$'$	=	precollision state
$''$	=	postcollision state
∞	=	freestream

Introduction

GAS flow around microscale structures forms an integral part of many applications of microelectromechanical systems (MEMS),[1] including microturbines, chemical sensors, micropropulsion for spacecraft, flow control devices, and gaseous chromatographs. Experimental study of microscale gas flows is made inherently difficult by the small physical dimensions and has been mainly limited to flows in simple microchannels and nozzles.[2,3] Although there have been a number of recent numerical studies of gas flows in microchannels,[4–6] there has been almost no investigation of gas flows over external bodies at microscale. This forms the subject of the present numerical investigation.

Gasdynamics can be classified into continuum, slip, transition, and free-molecular flow regimes. The basic parameter defining these regimes is the ratio of the molecular mean free path λ (at standard pressure and temperature, the mean free path of air is about 0.06 μm) to the smallest significant physical dimension characterizing the flow L (which can be around 1 μm or smaller for MEMS structures), namely, the Knudsen number ($Kn = \lambda/L$). For such flows, the Knudsen number may be larger than 0.01, which places the flow in the slip ($0.01 \leq Kn \leq 0.1$) or transition ($0.1 \leq Kn \leq 10$) regime. In these flows, the air in contact with the body surface may have a nonzero tangential velocity relative to the surface (slip), and collisions between molecules and collisions of the molecules with the wall have the same order of probability (transition). These rarefied phenomena must be included in any computer model designed to simulate these flow conditions.

Unfortunately, traditional computational fluid dynamics (CFD) techniques are only valid for the continuum regime ($Kn < 0.01$) and are acceptable for the slip regime if a slip wall condition is adopted instead of nonslip boundary condition. In general,

Presented as Paper 2001-3071 at the AIAA 35th Thermophysics Conference, Anaheim, CA, 11–14 June 2001; received 19 July 2001; revision received 19 November 2001; accepted for publication 3 December 2001.

*Graduate Student, Department of Aerospace Engineering. Student Member AIAA.
†Associate Professor, Department of Aerospace Engineering. Senior Member AIAA.
‡Professor, Department of Aerospace Engineering and Engineering Mechanics. Senior Member AIAA.

molecular-based numerical schemes, such as the direct simulation Monte Carlo (DSMC) method,[7] are more physically appropriate for rarefied gas flows at microscale. However, the disadvantages of the DSMC method are obvious for microflows.[8] It is very difficult for DSMC to isolate the useful signal from the noise in low-speed flows (microflows are usually low subsonic flows). The macroscopic flow velocity is sampled from the velocity of simulated microscopic particles ($V = V_i/N$) and the statistical scatter ($\sigma' = \sigma/\sqrt{N}, \sigma = \sqrt{(2RT)}$, where σ is about 400 m/s for air at standard temperature) is based on the sampling size. If we suppose the sample processes in DSMC are totally independent from step to step, then a sample size of 1.6×10^5 is needed to control the statistical scatter within 1 m/s and a sample size of 1.6×10^7 for the scatter to be within 0.1 m/s. Hence, few microflows can be simulated due to the limit of CPU time.[4]

An alternative approach is the information preservation (IP) method,[9] which is very effective in reducing the statistical scatter in the DSMC method for low-speed, constant density flow systems. The IP method preserves macroscopic information as well as microscopic information in simulated particles as the particles move and interact with each other and the domain boundaries. Recently, a two-dimensional IP code was implemented, and several cases were tested for low-speed isothermal flows.[6,10] We also implemented a two-dimensional IP code that is suitable for flows over external bodies at microscale based on a DSMC code.[11] In the new code, the macroscopic information is updated according to the inviscid fluid mechanics equations using the Lagrangian description, whereas collisions are considered between particles and with the body surface.

In this paper, the goal is to validate the IP code by simulating flows past a flat plate aligned with the freestream at low Reynolds numbers ($0.1 \le Re \le 100$). We also investigate the aerodynamics of a flat plate with thickness ratio of 5% at low Reynolds number ($Re = 4.0$) as a function of angle of attack using the IP method and a continuum approach with slip boundary conditions.

IP Method

It is generally required that each particle simulated in the DSMC method represents an enormous number (10^8–10^{25}) of real molecules, and these particles possess random thermal properties according to certain distributions (they are Maxwellian distributions for equilibrium gas flows). Hence, each particle has the microscopic information (molecular position, velocity, internal energy, etc.) and the collective information of the represented molecules (velocity, temperature, etc.). The information preservation method aims to preserve and update the collective information of the real molecules, intending to reduce the statistical scatter inherent in particle methods. In the paper by Fan and Shen,[12] information velocity was preserved and updated by collisions between particles, collisions of particles with the wall, and the external force field (the pressure field when gravity is neglected). Cai et al.[6] additionally preserved the number density information and velocity information for computational cells when the IP method was extended to two-dimensional isothermal problems. In our implementation,[13] number density information, velocity information, and temperature information for both particles and computational cells are preserved. The information is updated by collisions between particles, collisions of particles with a wall, and the inviscid fluid mechanics equations in the Lagrangian description.

An implementation of the IP method can be summarized as follows (see also Fig. 1):

1) All of the simulated particles and computational cells are assigned the necessary information after the computational domain is set up. For each particle, molecular velocity, location, and internal energy are assigned as in the DSMC method. The number density information, velocity information, and temperature information ($T_i = \langle C_i^2 \rangle / R, i = x, y, z$) are assigned to both particles and computational cells as the initial flow condition.

2) Move the particles using the molecular velocity with the same algorithms and models as the DSMC method.

3) In a time step Δt, the preserved information may be changed due to the following causes:

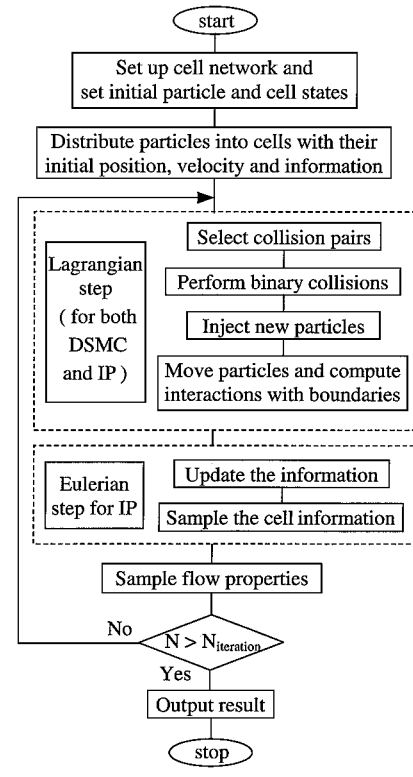

Fig. 1 DSMC-IP flowchart.

a) If there are collisions between particles, a simple scheme satisfying general conservation laws is employed to distribute the post-collision information for two collided particles. The preserved information of the two particles is set to be the same after collisions because collisions lead particles to be in an equilibrium state:

Conserved volume $\upsilon = 1/m \cdot n$,

$$1/n_1'' = 1/n_2'' = (1/n_1' + 1/n_2')/2 \tag{1}$$

Conserved momentum in x direction,

$$V_{x,1}'' = V_{x,2}'' = (V_{x,1}' + V_{x,2}')/2 \tag{2}$$

Conserved momentum in y direction,

$$V_{y,1}'' = V_{y,2}'' = (V_{y,1}' + V_{y,2}')/2 \tag{3}$$

Conserved energy,

$$\begin{aligned} T_{x,1}'' = T_{y,1}'' = T_{z,1}'' = T_{x,2}'' = T_{y,2}'' = T_{z,2}'' \\ = (T_{x,1}' + T_{y,1}' + T_{z,1}' + T_{x,2}' + T_{y,2}' + T_{z,2}')/6 \\ + (1/3R) \cdot \left[(V_{x,2}' - V_{x,1}')^2 + (V_{y,2}' - V_{y,1}')^2 \right] / 4 \end{aligned} \tag{4}$$

b) If there are collisions of particles with a wall, the preserved information of collided particles are set in accordance with the collective behavior of a large number of real molecules. Namely, the information of the particles is set as the wall condition if it is a diffuse reflection, whereas the information velocity component perpendicular to the wall is reversed if it is a specular reflection.

c) If particles reflect from a symmetric boundary, the information velocity component perpendicular to the symmetric boundary is reversed.

d) If there are new particles entering into the computational domain, their information is set as the boundary condition.

e) The preserved information of all particles are updated following the inviscid fluid mechanics equations in the Lagrangian description:

$$\frac{\mathrm{d}[1/n]}{\mathrm{d}t} = \frac{1}{n}\left[\frac{\partial V_x}{\partial x} + \frac{\partial V_y}{\partial y} \right] \tag{5}$$

$$\frac{\mathrm{d}V_x}{\mathrm{d}t} = -\frac{1}{n \cdot m}\frac{\partial p_x}{\partial x} \tag{6}$$

$$\frac{\mathrm{d}V_y}{\mathrm{d}t} = -\frac{1}{n \cdot m}\frac{\partial p_y}{\partial y} \tag{7}$$

$$\frac{\mathrm{d}\left[\frac{1}{2}R \cdot T_x + V_x^2/2\right]}{\mathrm{d}t} = -\frac{1}{n \cdot m}\frac{\partial [p_x \cdot V_x]}{\partial x} \tag{8}$$

$$\frac{\mathrm{d}\left[\frac{1}{2}R \cdot T_y + V_y^2/2\right]}{\mathrm{d}t} = -\frac{1}{n \cdot m}\frac{\partial [p_y \cdot V_y]}{\partial y} \tag{9}$$

$$p_i = n \cdot k \cdot T_i, \qquad i = x, y \tag{10}$$

In the preceding equations, $\mathrm{d}/\mathrm{d}t$ is the full derivative, and $\partial/\partial t$ is the partial derivative. However, it is difficult to calculate the derivatives of the information for discrete particles. The preserved information of the cell is then used when calculating the derivatives on the right-hand side of Eqs. (5–9) using Eq. (11). If the number density n on the right-hand side of Eqs. (5–9) is replaced by the ratio of the number of represented molecules in the cell to the volume of the cell, the conservation properties can still be guaranteed. Notice that the concept of number density is not good for a single particle, and so the number density information of a particle takes the value for the cell. The preceding equations are solved using a finite volume method. For example, Eq. (6) is solved as

$$V_x^{t+\Delta t} - V_x^t = -\frac{\Delta t}{n \cdot m}\oint_{\text{cell edges}} p_x \,\mathrm{d}y \Big/ \oint_{\text{cell edges}} \mathrm{d}x\,\mathrm{d}y \tag{11}$$

The information on the cell edges is linearly interpolated by the information of the neighboring cells.

4) The preserved information of computational cells is calculated from the particles:

$$\frac{1}{n_c} = \sum_{j=1}^{N_c}\left(\frac{1/n_j}{N_c}\right) \tag{12}$$

$$V_{i,c} = \sum_{j=1}^{N_c}\left(\frac{V_{i,j}}{N_c}\right), \qquad i = x, y \tag{13}$$

$$T_{i,c} = \sum_{j=1}^{N_c}\left(\frac{T_{i,j}}{N_c}\right), \qquad i = x, y, z \tag{14}$$

5) Macroscopic quantities are computed based on the preserved information. The macroscopic quantities are set to zero before sampling. For field data, those quantities are accumulated by adding the preserved information of the cell for every sampling step. Then the quantities divided by the number of sampling steps provide the final sampled macroscopic properties. For surface quantities, free-molecular theory is employed based on the pre- and postcollision information of particles collided with the wall because there is no collision between particles during this process. Equations (15) and (16) describe the pressure information and shear stress information for the collisions between particles and the wall. In these equations, erf ( ) is the error function. Approximately, T may be regarded as the average of the component temperatures in three directions. Like field quantities, surface quantities are sampled by sampling the information of collisions between particles and the wall for every incident particle. The final sampled surface properties are obtained as the accumulated surface quantities divided by the total number of incident particles:

$$p_i = n_i k T_i\left\{\left(s_3/\sqrt{\pi}\right)e^{-s_3^2} + \left(\tfrac{1}{2} + s_3^2\right)[1 + \mathrm{erf}(s_3)]\right\}$$

$$p_r = \tfrac{1}{2}n_i k T_i\sqrt{(T_r/T_i)}\left\{e^{-s_3^2} + \sqrt{\pi}s_3[1 + \mathrm{erf}(s_3)]\right\}$$

$$p = p_i + p_r, \qquad s_3 = V_3\sqrt{m/2kT_i} \tag{15}$$

$$\tau_i = n_i k T_i s_{t,i}\left\{e^{-s_3^2}/\sqrt{\pi} + s_3[1 + \mathrm{erf}(s_3)]\right\}$$

$$\tau_r = n_i k T_i s_{t,r}\left\{e^{-s_3^2}/\sqrt{\pi} + s_3[1 + \mathrm{erf}(s_3)]\right\}$$

$$\tau = \tau_i - \tau_r, \qquad s_{t,i\,\mathrm{or}\,r} = V_{t,i\,\mathrm{or}\,r}\sqrt{m/2kT_{i\,\mathrm{or}\,r}} \tag{16}$$

6) For steady flows, repeat steps 2–4 until the flow reaches a steady state. Then repeat steps 2–5 to sample and obtain the macroscopic quantities of the flow.

The preceding implementation of the IP method can greatly reduce the statistical scatter for low subsonic flows. In DSMC, the statistical scatter comes directly from the thermal movement of particles. In IP, the thermal movement of particles causes the statistical scatter only at the information level. Hence, the statistical scatter of the information cannot be larger than the variation of the information in the whole flowfield. Therefore, the IP method can greatly reduce the statistical scatter and, hence, the computational cost for low-speed flows. The simulation of many practical microscale gas flows becomes possible. Another advantage of the IP method is that the preserved information of computational cells has small statistical scatter, and this can help the application of effective boundary conditions for the DSMC method for low-speed flows. However, the IP method also has disadvantages. One is that the IP method requires more memory.[6] Another is that the current implementation of the IP method cannot recover the kinetic result for energy flux.[13] Additional models may be required to address this issue. However, for flows over external bodies at microscale, the temperature variation is not large, and this effect is negligible.

Continuum Approach with Slip Boundary Conditions

Few experimental data or theoretical results are available for external flows at low Reynolds number ($Re < 1 \times 10^2$). We seek to use a continuum approach with slip boundary conditions to compare with the IP method for low Reynolds number flows.

The continuum approach solves the compressible Navier–Stokes equations using a finite volume formulation. The fluxes are evaluated with a second-order accurate modified Steger–Warming flux-vector splitting approach (see Ref. 14), and an implicit Gauss–Seidel line-relaxation method is used for the time integration (see Ref. 14). At the low Reynolds numbers of interest in this work, the method converges to a steady state very slowly. However, with a large number of time steps (typically about 1,000,000), the calculations reach a steady-state result.

The slip boundary conditions are implemented with the use of the Maxwell-type slip velocity expression (see Ref. 15):

$$V_s = \frac{2-\theta}{\theta}\lambda\left.\frac{\partial V}{\partial n}\right|_w \tag{17}$$

where the mean free path λ is given by $\lambda = 2\mu/\rho\langle c\rangle$. We include a similar expression for the surface temperature slip, but at these low-speed conditions there is only a very small variation in temperature. Thus, the temperature slip is unimportant. The slip velocity in the direction tangent to the surface is computed with the preceding formula, and the normal direction velocity is set to zero. The accommodation coefficient θ is set to the same value as in the DSMC/IP calculations.

Numerical Simulation of Gas Flows over Flat Plates

In this section, we aim to investigate the aerodynamics of a flat plate airfoil with thickness ratio of 5% at low Reynolds number using the IP method and the continuum approach with slip boundary conditions. Before the investigation, the skin friction of a flat plate with zero thickness at low Reynolds number flows is compared among the IP method and other techniques, to check the validity of the IP implementation for flows over external bodies at the microscale.

Flow over a Flat Plate with Zero Thickness

The problem of rarefied flow past a two-dimensional flat plate aligned with the freestream is one of fundamental interest because

it generates a wide range of basic flow phenomena. As the Reynolds number decreases at a fixed Mach number, the nature of the flow changes from continuum to free molecular. Schaaf and Sherman[16] investigated flows over a flat plate experimentally and theoretically in the range of $3.4 \times 10^1 < Re < 2.02 \times 10^3$ for $2.5 < M < 3.8$ and $3 < Re < 5 \times 10^2$ for M about 0.2 and 0.6. Other theories[17–20] are also available for such flows from the slip regime to the free-molecular regime. However, theories for flows in the slip and transition regions can only predict flows qualitatively due to the approximations made. The IP method, on the other hand, is designed to simulate flows at different Reynolds number from free-molecular to near-continuum conditions.

Consider airflow past a flat plat with a finite length of 20 μm. The freestream velocity is about 69 m/s and the Mach number of the freestream is 0.2 with a temperature of 295 K. The freestream density is determined from the Reynolds number based on the length of the plate. Figure 2 shows the computational domain used in the simulation. The whole domain is divided into 4800 nonuniform structured cells that are clustered to the plate. On average, 50 particles are located in each cell. When the Reynolds number is larger than 10, a subcell technique is employed with more simulated particles in each cell. For each case, the time step is smaller than the mean collision time of molecules. Finally, the given results are sampled after the skin friction reaches a constant value.

Figure 3 shows the drag coefficient of the plate for both sides at low Reynolds numbers from several techniques. The IP results approach the free-molecular theory[21] ($C_D = 1.35/M$) when the Reynolds number becomes small ($Re < 0.2$) and is close to the numerical solutions of the full Navier–Stokes equations of incompressible flows[18] when the Reynolds number is greater than 10. DSMC results are also shown in Fig. 3. However, the DSMC simulations show larger statistical scatter when the Reynolds number is smaller. The following expression was derived by Tamada and Miura[19] for the flat plate drag coefficient in slip flow on the basis of Oseen–Stokes equations of motion:

$$C_D = \frac{8\pi}{R\{\ln(16/R) - \gamma + 1\}}\left\{1 - \frac{4k}{\pi}\frac{\ln(2/k) + \gamma + 1}{\ln(16/R) - \gamma + 1}\right\} \quad (18)$$

If we take k in Eq. (18) as the Knudsen number based on the length of the plate, the theory predicts similar results as the IP method for Reynolds number around 1 and 2. The experimental data from Schaaf and Sherman[16] shown in Fig. 3 were measured at a Mach number around 0.2, except that the case for the Reynolds number of 3.15 was measured with Mach number of 0.167. Good agreement is obtained between the experimental data and the IP results, except for Reynolds number of 3.15. The difference here occurs because the Mach number of the flow is another important parameter for the drag on the plate at low Reynolds number. The incompressible experimental data of Janour[22] are also plotted in Fig. 3. It seems when the Reynolds number is larger than 10, the difference between the results from the compressible and incompressible flow is very small. Obviously, the Blasius solution of the boundary layer theory (see Ref. 23) is not valid for low Reynolds number flows. To evaluate the implementation of the slip boundary conditions for the continuum approach, the results from this approach are also plotted in Fig. 3. As can be seen, the continuum approach predicts very good results when the Reynolds number is large than 10.

The local variation of skin friction over the plate is plotted in Fig. 4. The skin friction increases and approaches the free-molecular limit 3.375 ($C_f = 0.675/M$) as the Reynolds number decreases. This is quite different from the incompressible flow[18] where the combination of skin friction and the Reynolds number $C_f\sqrt{(Re_L)}$ increases from the Blasius solution to infinity when the Reynolds number decreases. Generally, there is an obvious effect of the leading edge and trailing edge on the skin friction. Both ends of the finite plate have larger skin friction than the average when the Reynolds number is larger than 1. In addition, the skin friction does not approach a constant value as the Reynolds number approaches zero. The slip velocity V_s (Fig. 5) on the plate shows similar behavior as the skin friction, which can be predicted by kinetic theory. If the plate is assumed as a fully momentum accommodated plate, the shear stress can be expressed as Eq. (19) from the implementation of the IP method:

$$\tau = \tfrac{1}{2}mn_i V_s\langle c\rangle\left\{e^{-s_3^2}/\sqrt{\pi} + s_3[1 + \mathrm{erf}(s_3)]\right\}$$

$$\langle c\rangle = \sqrt{8kT_i/\pi m} \quad (19)$$

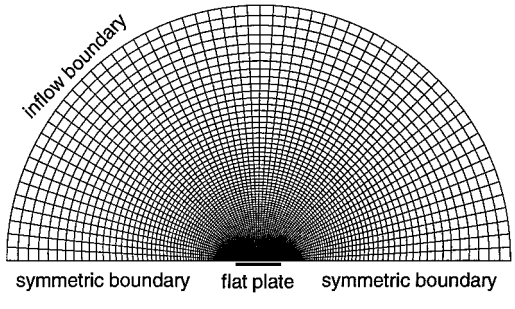

Fig. 2 Computational grid for flow over a flat plate with zero thickness.

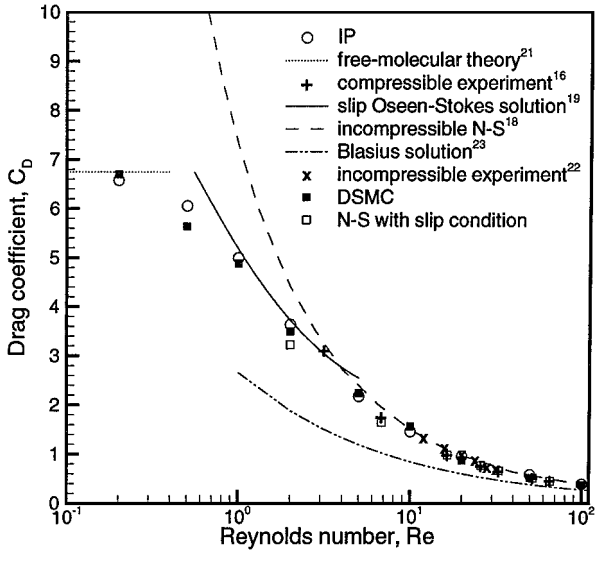

Fig. 3 Drag coefficient of a finite plate at low Reynolds numbers.

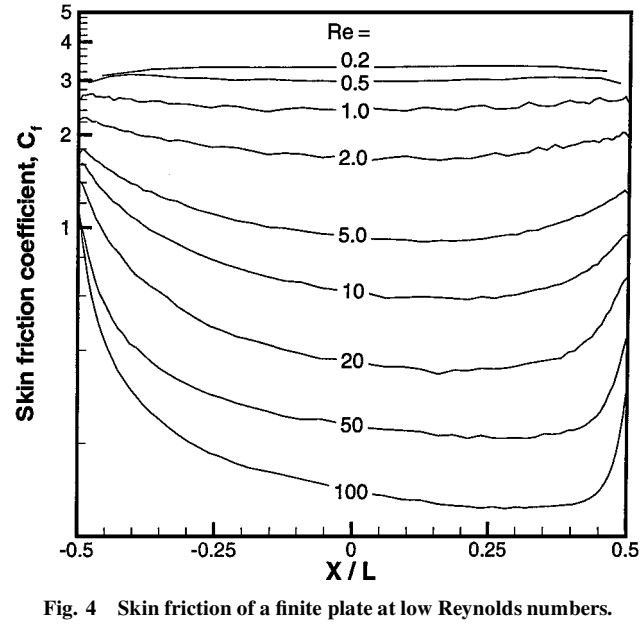

Fig. 4 Skin friction of a finite plate at low Reynolds numbers.

Table 1 Freestream conditions

Parameter	Value
M_∞	0.087
Re_∞	4.0
ρ_∞, kg/m^3	0.1216
T_∞, K	295
U_∞, m/s	30.0

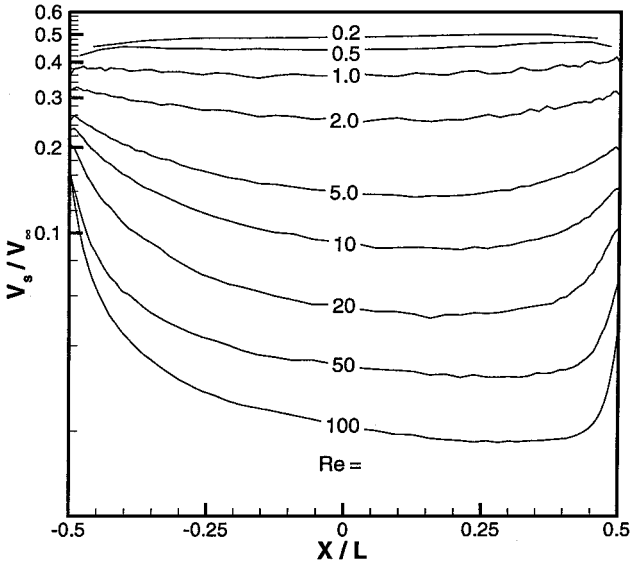

Fig. 5 Slip velocity of a finite plate at low Reynolds numbers.

For low-speed flows (if s is small, then s_3 is much smaller), the density variation and temperature variation are small, and so the skin friction can be approximated as Eq. (20). Hence, the skin friction is proportional to the slip velocity. For very low Reynolds number flows ($Re < 1.0$), the slip velocity also does not approach a constant value. This is because the ends of the plate act as stagnation points, so that the velocity is relatively small around the ends of the plate:

$$C_f = (\langle c \rangle / V_\infty) \cdot (V_s / V_\infty) \tag{20}$$

Flow over a Flat Plate with Thickness Ratio of 5%

The measurements of Sunada et al.[24] showed that a flat plate with thickness ratio of 5% had a much larger lift coefficient than NACA airfoils at $Re = 4 \times 10^3$ for incompressible flows. However, flows over microscale structures are usually at much lower Reynolds number. Hence, it is of interest to investigate the aerodynamics of a 5% flat plate at lower Reynolds number because the airfoil performance depends on the Reynolds number.

The 5% flat plate is placed at different angles of attack in an otherwise uniform stream of gas. The freestream condition is listed in Table 1, and the chord length of the plate is 20 μm. For the continuum approach with slip boundary conditions, an O grid of dimension 186 × 60 cells is used. The grid is exponentially stretched to the airfoil surface and extends 10 chord lengths from the airfoil surface. The grid is also stretched near the corners of the airfoil to resolve the large gradients there. Grid convergence studies were performed to verify that the results are grid independent. Figure 6 displays a part of the structured grid for the IP method from a computational domain that extends 5 chord lengths from the airfoil. For the IP method, a total of 11,200 cells is used, and about 50 particles are located in each cell. The total sampling size is about 5,000,000 particles per cell after 300,000 iterations are executed with a time step of 2×10^{-11} s. Figure 7 shows the pressure history at several locations along the plate for the case with a 10-deg angle of attack. With the given sampling size, the fluctuation of pressure is within

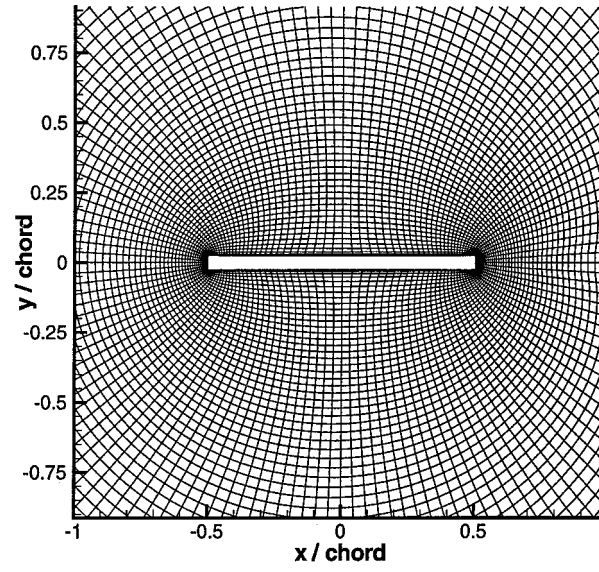

Fig. 6 Part of computational grids for flow over a flat plate with thickness ratio of 5%.

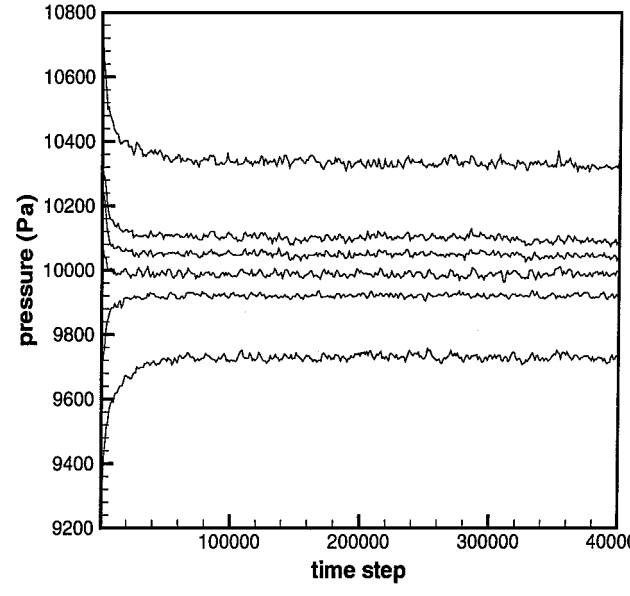

Fig. 7 Pressure history at several locations along the plate.

2 Pa, hence, the numerical error of the pressure coefficient is smaller than 0.04, or 4%.

Consider the case for the angle of attack of 10-deg. The pressure contours are plotted in Fig. 8 for both the IP method and the continuum approach. Figure 9 shows the velocity contours for both methods. Approximately speaking, the simulated flowfields from the two methods exhibit similar basic features. There is a high-pressure region around the leading edge and a low-pressure region around the trailing edge, which yields part of the drag on the plate. The pressure below the plate is higher than the pressure above the plate that generates the lift for the airfoil. The flow transfers part of its momentum to the plate, which decreases its velocity around the plate and increases the drag on the plate as another main factor. However, differences between the two solutions are also obvious. The variation of pressure from the IP method is smaller than that from the continuum approach. Namely, the pressure in the high-pressure region from the IP method is smaller than that from the continuum approach, and the pressure in the low-pressure region from the IP method is higher than that from the continuum approach. Also, the continuum approach predicts smaller velocities around the airfoil than the IP method does. These differences are much clearer from

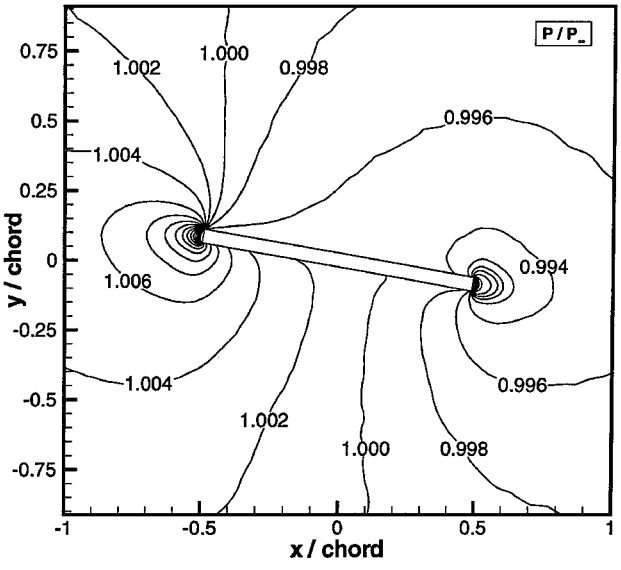

Fig. 8a Pressure field from the IP method.

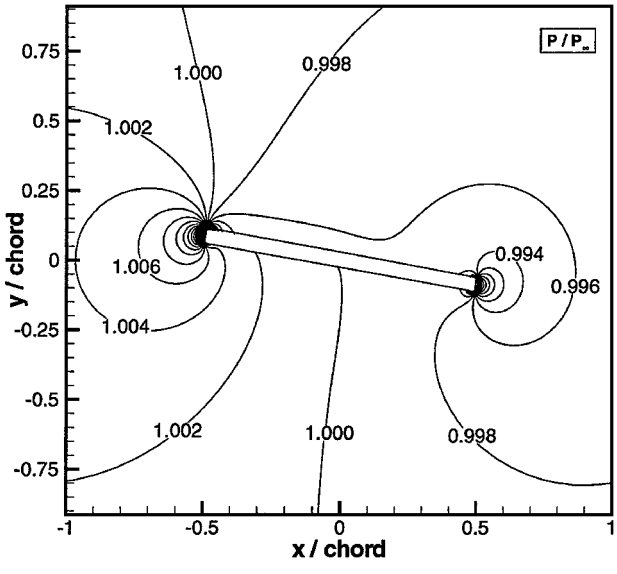

Fig. 8b Pressure field from the continuum approach.

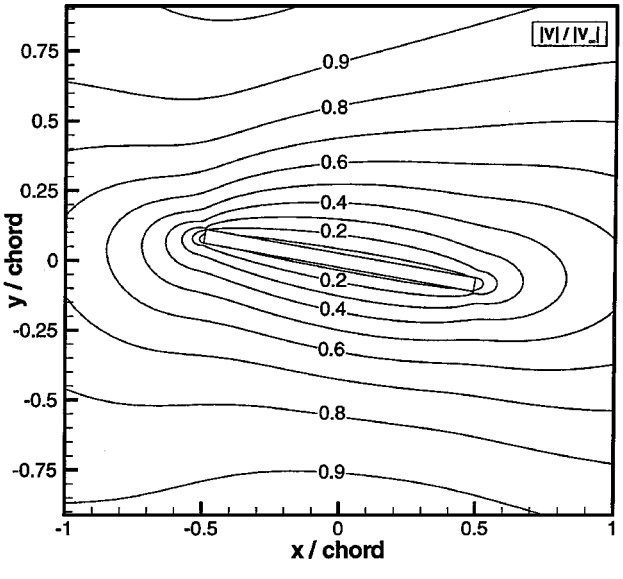

Fig. 9a Velocity field from the IP method.

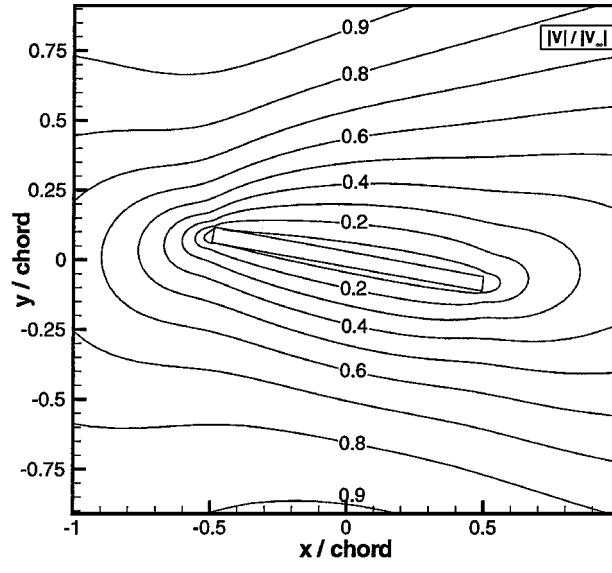

Fig. 9b Velocity field from the continuum approach.

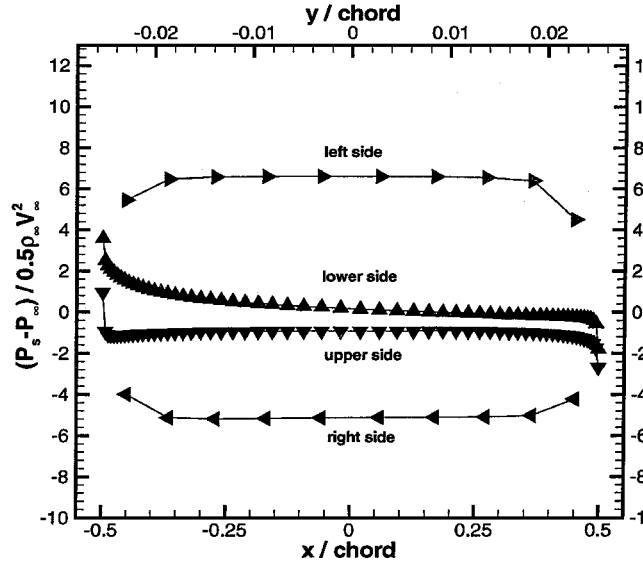

Fig. 10a Pressure distributions along the plate surface from the IP method.

the surface properties shown in Figs. 10 and 11. There is some difference of the pressure coefficient on the airfoil between the two solutions, and the shear stress on the airfoil from the IP method is much larger than that from the continuum approach.

Comparison is also made among the solutions from IP, DSMC, and continuum approach for the shear stress on both main sides of the plate (the sides of the plate are defined as left, right, lower, and upper side, according to its position when the angle of attack is zero). The DSMC results are much closer to the IP results than the continuum solutions, although the DSMC results exhibit large statistical scatter. Again, because of the large statistical scatter, the pressure coefficient distribution from the DSMC method is not shown here because 1% variation of the pressure will result in 2.0 variation of pressure coefficient. Unfortunately, there are no theoretical results for this airfoil at this Reynolds number, and the results here will eventually be compared with an experiment that is being planned.[25] To compare with the results in Fig. 3 when the freestream Mach number is 0.087, we consider the flow over the 5% plate with zero angle of attack. The average skin friction for the 5% flat plate is about 1.37 from the IP method, and it is about 1.52 for the plate with zero thickness. (This value is larger than 1.26 from Fig. 3 when $Re = 4.0$ because the Mach number is decreased.) The average

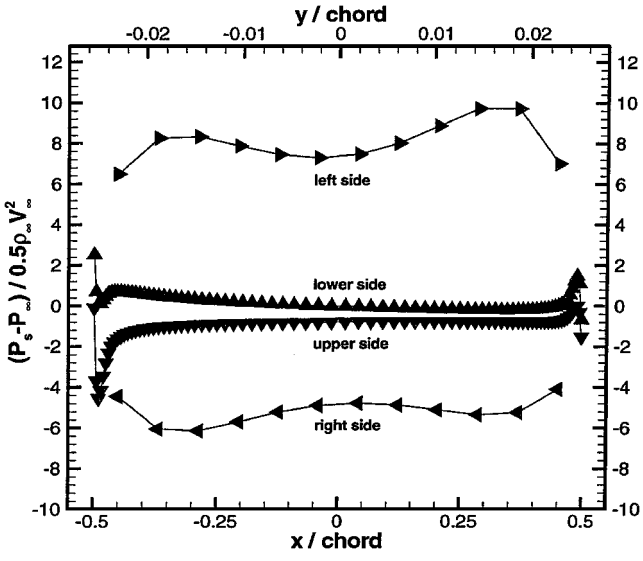

Fig. 10b Pressure distributions along the plate surface from the continuum approach.

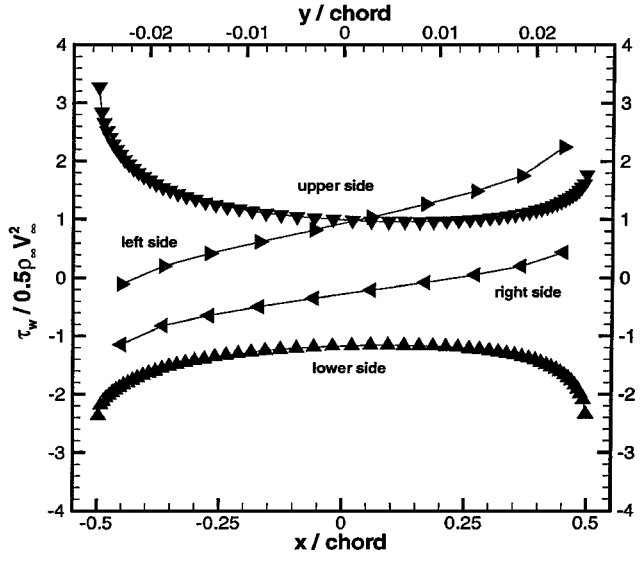

Fig. 11a Skin-friction distributions along the plate surface from the IP method.

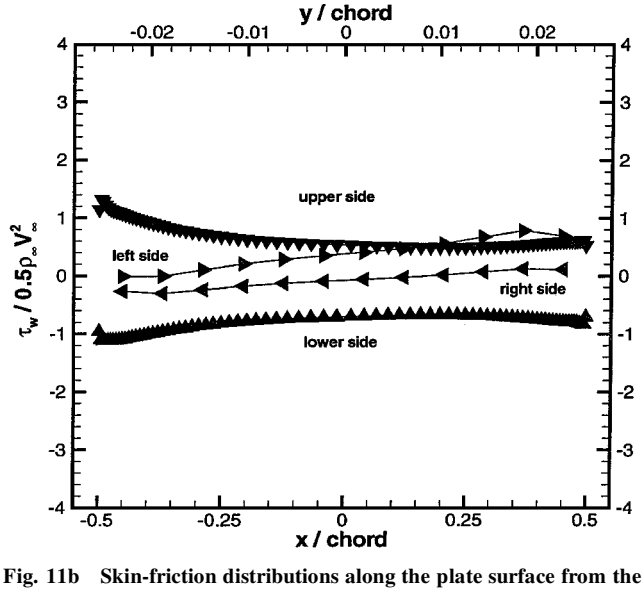

Fig. 11b Skin-friction distributions along the plate surface from the continuum approach.

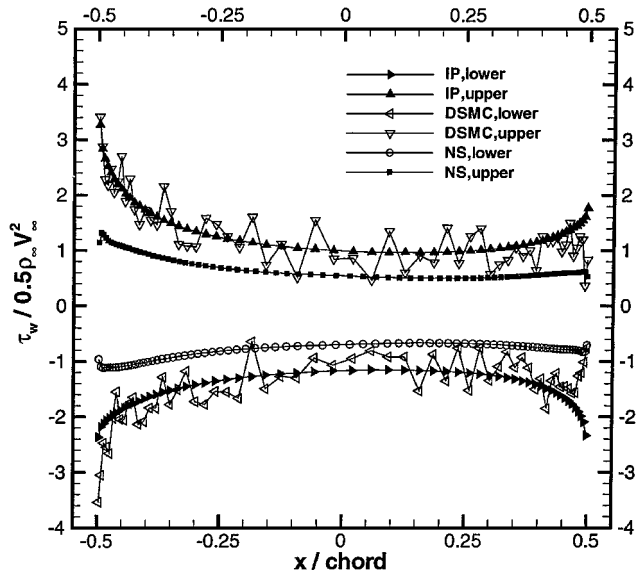

Fig. 11c Skin-friction distributions on the plate surface from three methods.

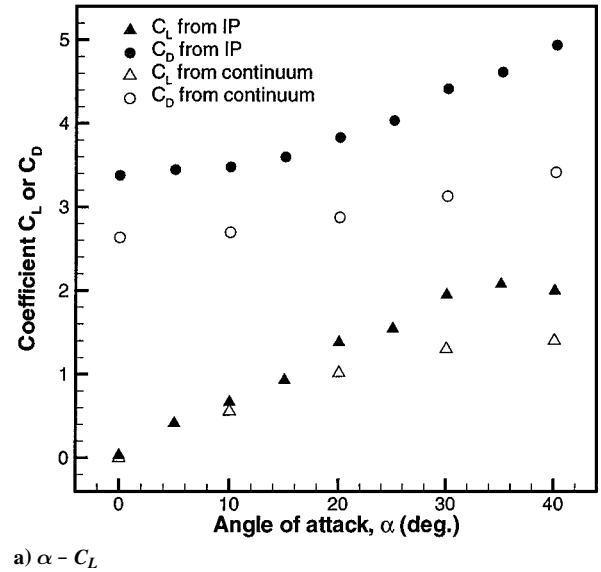

a) $\alpha - C_L$

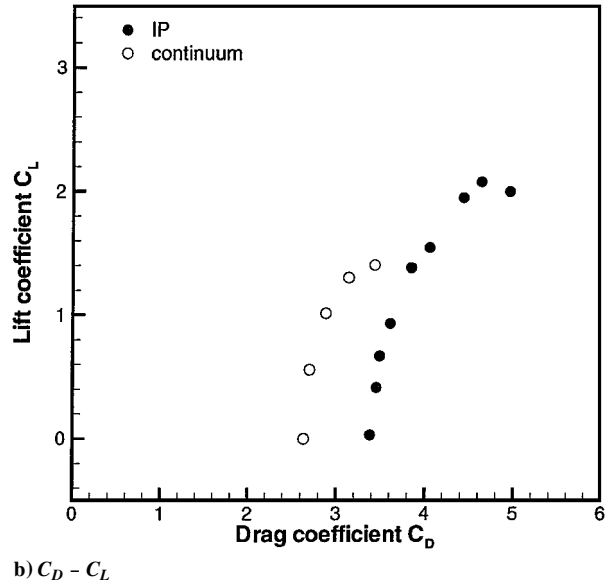

b) $C_D - C_L$

Fig. 12 Characteristics of 5% flat plate at $Re = 4.0$.

skin friction from the continuum approach, however, is too small at about 0.81. We also notice that the thickness of the plate will affect the skin friction on the surface. For free-molecular flow, the ratio of the drag on the 5% flat plate ($C_D = 18.29$) to the drag on the plate with zero thickness ($C_D = 15.51$) is about 1.18. When the Reynolds number is 4×10^3, the ratio of the drag on the 5% flat plate ($C_D = 0.057$, Ref. 24) to the drag on the plate with zero thickness ($C_D = 0.0478$, Ref. 18) is about 1.19. When the measurement errors ($\pm 9\%$) in the Sunada et al. experiment[24] are considered, then the ratio ranges from 1.08 to 1.30. Also, when the Reynolds number is 4.0, the ratio of the drag on the 5% plate ($C_D = 3.38$, IP) to the drag on the plate with zero thickness ($C_D = 3.04$, IP) is about 1.11. This is a reasonable value compared with the free-molecular theory and the experimental data. Again, the drag coefficient on the 5% plate from the continuum approach is too small at about 2.63. It may be that the slip boundary conditions as implemented are not appropriate for these flows. Perhaps additional terms must be incorporated into the Navier–Stokes equations, such as the Burnett equations. Another possible reason is that the continuum approach is not valid for a very small region, for example at the body surface, but this affects the whole flow because the equations are elliptic.

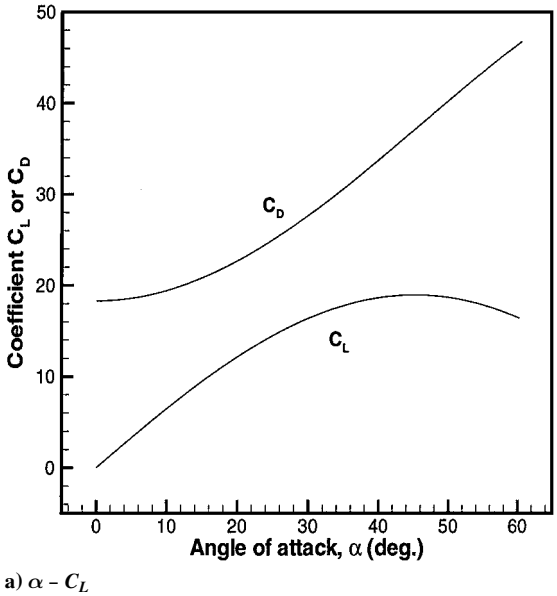

a) $\alpha - C_L$

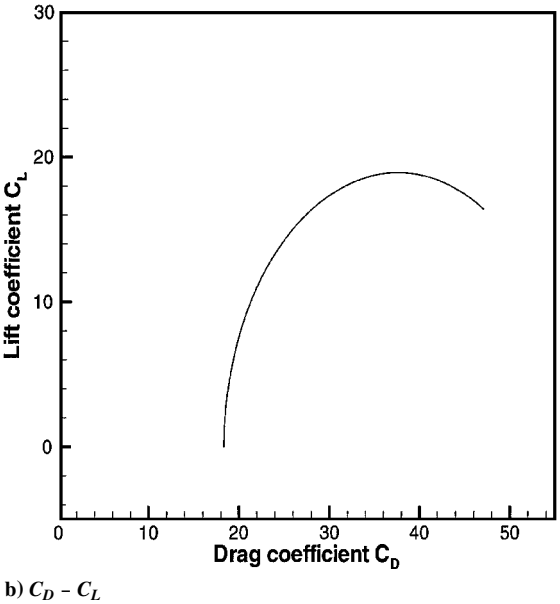

b) $C_D - C_L$

Fig. 13 Characteristics of 5% flat plate at $Re \sim 0$ from free-molecular theory.

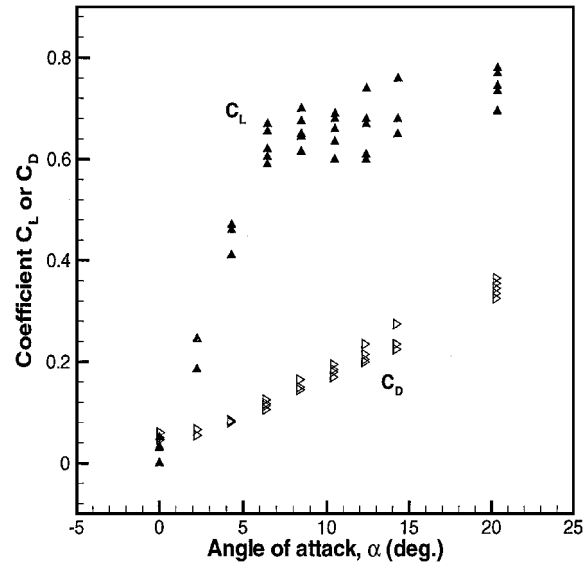

a) $\alpha - C_L$

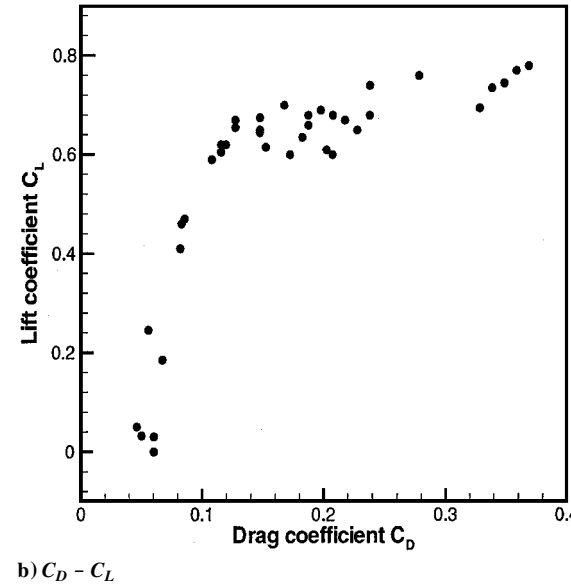

b) $C_D - C_L$

Fig. 14 Characteristics of 5% flat plate at $Re = 4 \times 10^3$ from the experiment.

The aerodynamic characteristics of the 5% flat plate are plotted in Figs. 12a and 12b when the Reynolds number is 4. For comparison, the aerodynamics of the plate is plotted in Figs. 13a and 13b for free-molecular flows and in Figs. 14a and 14b when the Reynolds number is 4×10^3 (Ref. 24). Clearly, the aerodynamics at $Re = 4$ is closer to that of free-molecular flow than that when $Re = 4 \times 10^3$ although the values are much smaller. The ratio of lift to drag is less than 1 when $Re = 4$, which agrees with Miyagi's result.[26] From the IP results, the lift slope is about 3.82, which is smaller than 5.8 when $Re = 4 \times 10^3$. The same trend exists for NACA0009 airfoil at higher Reynolds numbers[24] with 2.9 at $Re = 4 \times 10^3$ and 5.5 at 4×10^4.

Conclusions

The information preservation method is used to investigate gas flows over microscale airfoils under conditions that range from near-continuum flow to transition flow. Good agreement is obtained between the IP method and other data (both experimental and computational) for the drag on a flat plate with zero thickness in low Reynolds number flows across all flow regimes.

The aerodynamics of a flat plate with a thickness ratio of 5% at $Re = 4$ was investigated numerically and found to be quite different from that at $Re = 4 \times 10^3$. The lift slope of the plate at Reynolds

number of 4 is about 3.82, and the ratio of lift to drag is less than 1. This may be one reason that small insects flap their wings to increase lift. In addition, the continuum approach with slip boundary conditions predicts similar basic flow patterns as the IP method, but there are differences in details. This may indicate that continuum approaches are not suitable for this kind of flow because of rarefied effects. It may be necessary to incorporate additional terms into the Navier–Stokes equations to address this problem.

Acknowledgment

This work was supported by the Air Force Office of Scientific Research through the Multidisciplinary Research Program of the University Research Initiative Grant F49620-98-1-0433.

References

[1]Ho, C. M., and Tai, Y. C., "Micro-Electro-Mechanical-Systems (MEMS) and Fluid Flows," *Annual Review of Fluid Mechanics*, Vol. 30, 1998, pp. 579–612.

[2]Pong, K. C., Ho, C. M., Liu, J., and Tai, Y. C., "Non-Linear Pressure Distribution in Uniform Microchannels," *Application of Microfabrication to Fluid Mechanics*, Vol. 197, American Society of Mechanical Engineers, Fairfield, NJ, 1994, pp. 51–56.

[3]Arkilic, E., Schmidt, M. A., and Breuer, K. S., "Gaseous Slip Flow in Long Microchannels," *Journal of Micro Electro Mechanical Systems*, Vol. 6, No. 2, 1997, pp. 167–178.

[4]Oh, C. K., Oran, E. S., and Cybyk, B. Z., "Microchannel Flow Computed with the Discrete Simulation Monte Carlo–MLG," AIAA Paper 95-2090, June 1995.

[5]Mavriplis, C., Ahn, J. C., and Goulard, R., "Heat Transfer and Flowfields in Short Microchannels Using Direct Simulation Monte Carlo," *Journal of Thermophysics and Heat Transfer*, Vol. 11, No. 4, 1997, pp. 489–496.

[6]Cai, C., Boyd, I. D., Fan, J., and Candler, G. V., "Direct Simulation Method for Low-Speed Microchannel Flows," *Journal of Thermophysics and Heat Transfer*, Vol. 14, No. 3, 2000, pp. 368–378.

[7]Bird, G. A., *Molecular Gas Dynamics and the Direct Simulation of Gas Flows*, Oxford Science, New York, 1994.

[8]Beskok, A., "Physical Challenges and Simulation of Micro Fluidic Transport," AIAA Paper 2001-0718, Jan. 2001.

[9]Fan, J., and Shen, C., "Statistical Simulation of Low-Speed Rarefied Gas Flows," *Journal of Computational Physics*, Vol. 167, No. 2, 2001, pp. 393–412.

[10]Fan, J., Boyd, I. D., Cai, C. P., Hennighausen, K., and Candler, G. V., "Computation of Rarefied Gas Flows Around a NACA 0012 Airfoil," *AIAA Journal*, Vol. 39, No. 4, 2001, pp. 618–625.

[11]Dietrich, S., and Boyd, I. D., "Scalar and Parallel Optimized Implementation of the Direct Simulation Monte Carlo Method," *Journal of Computational Physics*, Vol. 126, No. 2, 1996, pp. 328–342.

[12]Fan, J., and Shen, C., "Statistical Simulation of Low-Speed Unidirectional Flows in Transition Regime," *Rarefied Gas Dynamics*, Vol. 2, 1999, pp. 245–252.

[13]Boyd, I. D., and Sun, Q., "Particle Simulation of Microscale Gas Flows," AIAA Paper 2001-0876, Jan. 2001.

[14]MacCormack, R. W., and Candler, G. V., "The Solution of the Navier–Stokes Equations Using Gauss–Seidel Line Relaxation," *Computers and Fluids*, Vol. 17, No. 1, 1989, pp. 135–150.

[15]Schaaf, S. A., and Chambre, P. L., "Flow of Rarefied Gases," *High Speed Aerodynamics and Jet Propulsion*, Vol. 3, No. H, 1958, pp. 678–739.

[16]Schaaf, S. A., and Sherman, F. S., "Skin Friction in Slip Flow," *Journal of the Aeronautical Sciences*, Vol. 21, No. 2, 1954, pp. 85–90.

[17]Mirels, H., "Estimate of Slip Effect on Compressible Laminar-Boundary-Layer Skin Friction," NACA TN 2609, 1951.

[18]Dennis, S. C., and Dunwoody, J., "The Steady Flow of a Viscous Fluid past a Flat Plate," *Journal of Fluid Mechanics*, Vol. 24, 1966, pp. 577–595.

[19]Tamada, K., and Miura, H., "Slip Flow past a Tangential Flat Plate at Low Reynolds Numbers," *Journal of Fluid Mechanics*, Vol. 85, 1978, pp. 731–7427.

[20]Liu, V. C., "On the Drag of a Flat Plate at Zero Incidence in Almost-Free-Molecule Flow," *Journal of Fluid Mechanics*, Vol. 5, 1959, pp. 481–496.

[21]Gombosi, T. I., *Gaskinetics Theory*, Cambridge Univ. Press, Cambridge, England, U.K., 1994, pp. 227–261.

[22]Janour, Z., "Resistance of a Plate in Parallel Flow at Low Reynolds Numbers," NACA TM 1316, 1951.

[23]Churchill, S. W., "Viscous Flows: The Practical Use of the Theory," Butterworths, Stoneham, England, U.K., 1988, pp. 255–269.

[24]Sunada, S., Sakaguchi, A., and Jawachi, K., "Airfoil Section Characteristics at a Low Reynolds Number," *Journal of Fluids Engineering*, Vol. 119, No. 1, 1997, pp. 129–135.

[25]Martin, M. J., Kurabayashi, K., and Boyd, I. D., "Measurement of Lift and Drag on MEMS Scale Airfoils in Slip Flow," *Proceedings of 2001 ASME Fluids Engineering Division Summer Meeting*, Vol. 1, American Society of Mechanical Engineers, Fairfield, NJ, 2001, pp. 763–768.

[26]Miyagi, T., "Oseen Flow past a Flat Plate Inclined to the Uniform Stream," *Journal of the Physical Society of Japan*, Vol. 19, No. 6, 1964, pp. 1063–1073.